JAAS

Accepted Manuscript

This is an *Accepted Manuscript*, which has been through the Royal Society of Chemistry peer review process and has been accepted for publication.

Accepted Manuscripts are published online shortly after acceptance, before technical editing, formatting and proof reading. Using this free service, authors can make their results available to the community, in citable form, before we publish the edited article. We will replace this *Accepted Manuscript* with the edited and formatted *Advance Article* as soon as it is available.

You can find more information about *Accepted Manuscripts* in the Information for Authors.

Please note that technical editing may introduce minor changes to the text and/or graphics, which may alter content. The journal's standard Terms & Conditions and the Ethical guidelines still apply. In no event shall the Royal Society of Chemistry be held responsible for any errors or omissions in this *Accepted Manuscript* or any consequences arising from the use of any information it contains.

ROYAL SOCIETY OF CHEMISTRY

www.rsc.org/jaas

Journal Name

ARTICLE TYPE

Cite this: DOI: 10.1039/xxxxxxxxxx

Chemical speciation via X-ray emission spectroscopy in the tender X-ray range

Marko Petric[a,b] and Matjaž Kavčič[a]

Received Date
Accepted Date

DOI: 10.1039/xxxxxxxxxx

www.rsc.org/journalname

The $K\alpha$ X-ray emission spectra from a series of phosphorus, sulfur, and chlorine containing compounds covering the full range of oxidation states were measured employing high energy resolution proton induced X-ray emission (PIXE) spectroscopy in the tender x-ray range. Measurements were accompanied by the quantum chemistry calculations based on the density functional theory (DFT). Clear energy shifts of the $K\alpha$ lines were measured in correlation with the formal oxidation state for all three elements. This correlation was improved even further using the effective charge based on the DFT calculated valence electron population. Finally, it is demonstrated that the oxidation state analysis based on the $K\alpha$ energy shifts can be used also for a quantitative analysis of the proportion of separate low-Z species in mixed valence systems.

1 Introduction

Chemical speciation is of fundamental importance in various research fields such as material and environmental science, biology, geology, chemistry, and others. Inner shell X-ray spectroscopies provide experimental information on the electronic structure of particular element in bulk material and are nowadays carried on almost routinely at the third generation synchrotron sources. In case of X-ray absorption spectroscopy (XAS) transitions of core electron into the unoccupied states above the Fermi level are probed, while in X-ray emission spectroscopy (XES) we are studying the relaxation of the core-ionized atom by a radiative transition from the occupied electronic states below the Fermi level. Both techniques provides complementary information on the electronic structure and can be used to perform chemical speciation. However, there is one important conceptual difference between the two. While XAS spectroscopy relies on the use of monochromatic tunable X-ray source, XES is based on a second order process and is therefore not restricted to synchrotron facilities but can be used also in combination with laboratory excitation sources.

Commonly, high resolution XES spectroscopy is based on the use of crystal spectrometers which provide energy resolution in the emission channel comparable to the resolution of the synchrotron beamline monochromator. In order to enlarge the solid angle and enhance the collection efficiency, multiple analyzer focusing crystals are usually employed in the advanced hard X-ray emission spectrometers [1–6]. Because of multiple crystals and large target-detector distances needed to achieve high resolving power, these instruments are usually quite large and consequently operate in air. While these powerful high-resolution spectrometers are successfully employed to perform XES and also resonant inelastic X-ray scattering (RIXS) studies in the hard X-ray range the absorption sets their low energy working limit and they are not applicable for chemical speciation of low-Z elements with emission energies in the tender X-ray range (2-5 keV) requiring a full in-vacuum spectrometer [7].

In the last decade large progress have been made in the development of energy dispersive microcalorimeter X-ray detectors based on transition edge sensors which can be used alternatively to perform high resolution X-ray emission spectroscopy [8–10]. However, at the moment the energy resolution of this new generation X-ray detectors can still not match the resolution of good crystal spectrometers which is mandatory to address tiny chemical shifts studied in this work.

P, S, and Cl represent three extremely important elements with characteristic emission energies in the tender X-ray range. Because of their multivalent character they form chemical bonds with many atoms of different electronegativity influencing the local electronic structure around the center atom. So far X-ray absorption near edge spectroscopy (XANES) has been used predominantly to specify chemically these elements for example in minerals [11], sediments [12], silicate glasses [13], old pigments [14] and in Li-S batteries [15]. However, our recent XAS/XES comparative study on sulfur [16] demonstrated high sensitivity and selectivity of $K\alpha$ XES to the electronic charge making it a robust and efficient method for chemical characterization of sulfur. The same approach could be applied also to other neighboring elements making it a gener-

[a] Jozef Stefan Institute, Jamova 39, SI-1000 Ljubljana, Slovenia; E-mail: matjaz.kavcic@ijs.si
[b] Jozef Stefan International Postgraduate School, Jamova cesta 39, 1000 Ljubljana, Slovenia; E-mail: mpetric@ijs.si

ally applicable tool.

In this work our high energy resolution tender X-ray emission spectrometer[7] has been combined with the particle induced X-ray emission (PIXE) technique employing MeV proton beams to address chemical speciation of P, S, and Cl using high energy resolution $K\alpha$ X-ray emission spectra. High energy resoution PIXE (HR-PIXE) technique has been already used before by different authors for example to determine oxidation states in different phosphorus[17–19] and sulfur[20,21] compounds. It was applied to specify oxidation state of S and Cl in aerosol samples[20,22–24] and P in lake sediments[18]. All of these studies were based on an empirical approach using comparison with measured standards. In this work we are providing a more general absolute approach which can be applied to determine oxidation state of low-Z elements such as P, S, and Cl. A series of $K\alpha$ X-ray emission spectra on standard P, S and Cl compounds covering full range of oxidation states have been recorded. Our experimental energy resolution was below the natural lifetime broadening which allowed us to extract energy shift of $K\alpha$ line with high precision. Measurements were accompanied with the *ab-initio* quantum chemical calculations based on density functional theory (DFT) yielding effective valence-shell configuration and local electronic charge. Very high correlation of $K\alpha$ emission energy with local electronic charge was obtained for all three elements which provides a base for a true quantitative analysis of the oxidation state of the element in the sample.

2 Experimental

The high-energy resolution PIXE measurements were performed at the 2 MV tandem accelerator of the J. Stefan Institute, Ljubljana. Target pellets pressed from powder reference materials were mounted on a motorized disc shaped sample holder used to exchange targets without breaking the vacuum in the chamber. The target holder was tilted at an angle of 45^o with respect to the incident beam. The X-ray target emission was induced with 2 MeV protons, a broad unfocused proton beam with 8×8 mm^2 cross section was used and the proton current was in the range of 50-100 nA. The proton beam induced $K\alpha$ X-ray emission spectra were collected in the direction perpendicular to the incident beam by an in-vacuum Johansson-type single crystal spectrometer for high energy resolution X-ray emission spectroscopy in the tender X-ray range[7]. In case of phosphorus targets the first order reflection by the $(10\bar{1}0)$ plane of the SiO_2 crystal ($2d = 8.510\AA$) was used, while the first-order reflection of a Si(111) crystal ($2d = 6.271\AA$) was used for the sulfur and chlorine measurements. In order to achieve dispersive mode of operation, small modification of standard Johansson geometry has been done by moving the target holder inside the Rowland circle at the distance of 42 cm from the analyzer crystal. The diffracted photons were detected by a charged coupled device (CCD) detector, which was thermoelectrically cooled to -40 °C. The CCD detector consisted of 770×1152 pixels with 22.5×22.5 μm^2 pixel size. The position spectra recorded by the CCD detector were converted into energy scale relative to the position of the $K\alpha_1$ line of the K_3PO_4, pure S, and NaCl compound targets which served as references, with corresponding reference emission energies of 2014.54 eV[25], 2307.89 eV[26], and 2622.44 eV[26], respectively. The energy bandwidths covered by the CCD at fixed detector position were 44 eV, 28 eV, and 53 eV for P, S, and Cl $K\alpha$ measurements, respectively. The whole $K\alpha$ emission spectra for each element were therefore recorded simultaneously keeping the crystal and detector at fixed position during the measurement.

The final energy resolution of the spectrometer given as the FWHM of the instrumental response function was between 0.50 - 0.60 eV, depending on the Bragg angle corresponding to each of three measured elements. At these angles the geometrical contributions due to pixel size of the CCD detector and the vertical beam spot size are practically negligible and the width of the instrumental response was determined mainly by the intrinsic crystal broadening[7]. At this experimental resolution combined with good statistics in the measured spectra the fitting error of the measured energy shifts were between 1-2 meV. Because of simultaneous collection of full spectrum at fixed given crystal-detector position any possible errors introduced by limited precision of the motors used to move the crystal and detector are completely avoided. The main source of uncertainty originate from slight random variations in actual target position relative to the crystal which are introduced during target exchange and might lead to tiny shifts of the line on the detector. In order to determine this contribution independent measurements of several target pellets prepared out of same chemical compound were performed. These targets were mounted on different positions on the sample holder which was used to exchange between the targets in exactly the same way as during our measurements of different compound targets. The final experimental uncertainty was determined as a standard deviation of absolute position of the measured line within the detector yielding value of 0.40 detector channels. The latter was converted into energy using corresponding Bragg angles yielding final energy uncertainties of 23 meV, 15 meV, and 27 meV for P, S, and Cl measurements, respectively.

The count rate at the top of the $K\alpha_1$ line was with the SiO_2 analyzer crystal used to measure phosphorus compounds around 2 counts/sec and the acquisition time for single target was 2000 sec. Changing to Si(111) crystal for the measurements of S and Cl compounds the count rate increased to around 10 counts/sec and the overall acquisition time per target was reduced to 500 sec.

3 Theory

In order to interpret properly the measured energy shifts and provide the ground for true quantitative analysis of the oxidation state the *ab-initio* quantum chemical calculations were performed using the StoBe-deMon[27] molecular cluster package based on the density functional theory (DFT)[28]. First, the geometry optimization was performed yielding the ground state of each molecule. This was followed by the Mulliken population analysis[29–32] providing the character of molecular orbitals in terms of atomic orbitals. This population analysis assigns partial charges to the atoms and is used to study charge distribution within a molecule. In next step, geometrically optimized coordinates around centre P, S, or Cl atom were further on used to calculate the initial $1s^{-1}$ core-hole state and the final $2p^{-1}$ state, both were represented by

Kohn-Sham orbitals of the ground state[33,34]. The dipole transition moments were calculated as an explicit one-electron transitions. In order to improve further the accuracy of calculated transition energies individual optimization of initial and final states were performed and the final transition energies corresponding to $K\alpha$ emission were calculated as differences in orbital energies of separately optimized initial and final states. The GGA exchange functional by Becke, Be88[35], and the GGA correlation functional by Perdew, PD91[36,37] were used for exchange-correlation part. The same orbital basis set TZVP (73111/6111/1) was used for P, S and Cl atoms, respectively.

4 Results

For each of three elements studied in our work two measured $K\alpha_{1,2}$ spectra corresponding to compounds with the highest and the lowest formal oxidation number are presented in Figure 1. The high experimental resolution on the level of natural lifetime broadening allows one to observe tiny energy shifts of the measured $K\alpha$ emission lines depending on the oxidation state of the element in the sample. The experimental $K\alpha_{1,2}$ emission energies were extracted by fitting the measured spectra with two Voigt functions, which is a convolution of the natural Lorentzian shape with the Gaussian function corresponding to the instrumental function of the spectrometer. For both spectral components the corresponding Lorentzian and Gaussian components were constrained to the same values. Within the energy bandwidth covered by the detector additional spectral contribution is observed on the high energy side of the $K\alpha$ diagram line corresponding to the 1s→2p transitions in KL doubly ionized atom. Two additional Voigt profiles were added in the model spectrum to account for the $K\alpha_{3,4}$ components of the multiple ionization satellite line and such fitting model reproduced almost perfectly the measured spectra as presented in Figure 2. The final experimental $K\alpha$ emission energies extracted from the fit are tabulated in Table 1 for all measured compounds. The experimental 2p level spin orbit splitting was found 0.864(5), 1.180(11), and 1.592(15) eV for the case of P, S and Cl compounds, respectively, and show no dependence on the chemical state so only experimental $K\alpha_1$ emission energies are reported in Table 1.

From the tabulated values a clear trend is observed for measured compounds of all three elements. The $K\alpha$ line is shifted towards higher emission energy with increasing formal oxidation state. In Figure 3 the experimental $K\alpha_1$ emission energies are plotted versus formal oxidation state for each of three elements studied in this work and a high correlation is observed. Besides experimental energy values also DFT theoretical energies are added on Figure 3. The latter were all calculated with StoBe-deMon program, the molecular structure with first two coordination spheres around the atom of interest were included in the calculations. Since we could not achieve convergence for every measured system only calculations for several representative samples are presented. An overall shift of -1.13 eV (P), +0.77 eV (S), and +3.34 eV (Cl) were applied to the absolute calculated values in order to reach good agreement with the experiment. Most importantly, also the theory confirmed clearly the correlation of $K\alpha$ emission energies with the oxidation state as observed in experiment.

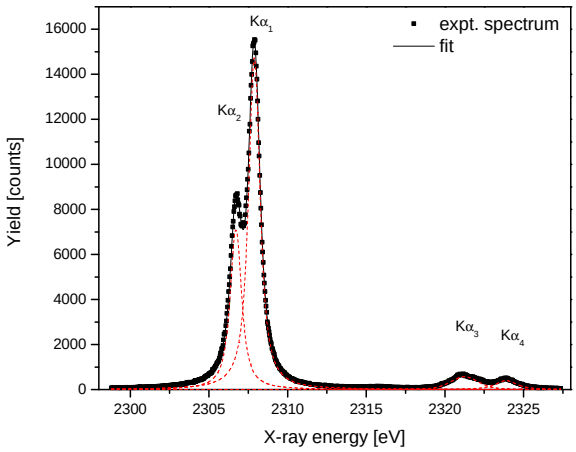

Fig. 2 High energy resolution $K\alpha$ X-ray emission spectrum of pure S target decomposed by the fitting model. Besides the $K\alpha_{1,2}$ diagram line also the $K\alpha_{3,4}$ satellite contributions corresponding to KL double ionization are observed on the high energy side of the spectrum.

The valence electron population which of course varies in different chemical compounds therefore affects slightly the screening of the nuclear potential experienced by core electrons producing chemical shifts. These shifts depend on the oxidation state confirmed by our experimental and theoretical values. On the other hand, measured energies for different compounds with the same oxidation state tabulated in Table 1 basically match each other indicating similar valence electron configuration. One small exception is the $Al(PO_3)_3$ exhibiting slightly higher energy compared to other P(5+) compounds but this was already explained in our previous work[19] focused on P with the large Al electronegativity compared to other metal ligands increasing slightly the phosphorus effective charge. Here we would like to study in more details the case of Na_2SO_3 and $Na_2S_2O_5$ compounds, both with formal oxidation state (4+) which exhibit difference in measured $K\alpha$ emission energy of 0.12 eV, which is significant compared to scattering of measured energies within other compounds of the same oxidation number. Intuitively, we can try to describe this difference just by looking into the chemical formulas for both samples under consideration. The numbers of oxygen atoms per single S atom is larger in Na_2SO_3 compared to $Na_2S_2O_5$. Because of large electronegativity of oxygen atoms a slight increase of the local electronic charge of the sulfur atom in $Na_2S_2O_5$ would be expected yielding slightly lower $K\alpha$ emission energy in agreement with our measurements.

A more thorough and explicit explanation is provided by the theory which enable us to determine small differences in effective electronic charge of compounds with the same oxidation state by studying their valence electron population. The latter was obtained by Mulliken analysis on the DFT calculated ground state electron density. The results of such analysis are presented in Table 2 for several representative compounds of each three ele-

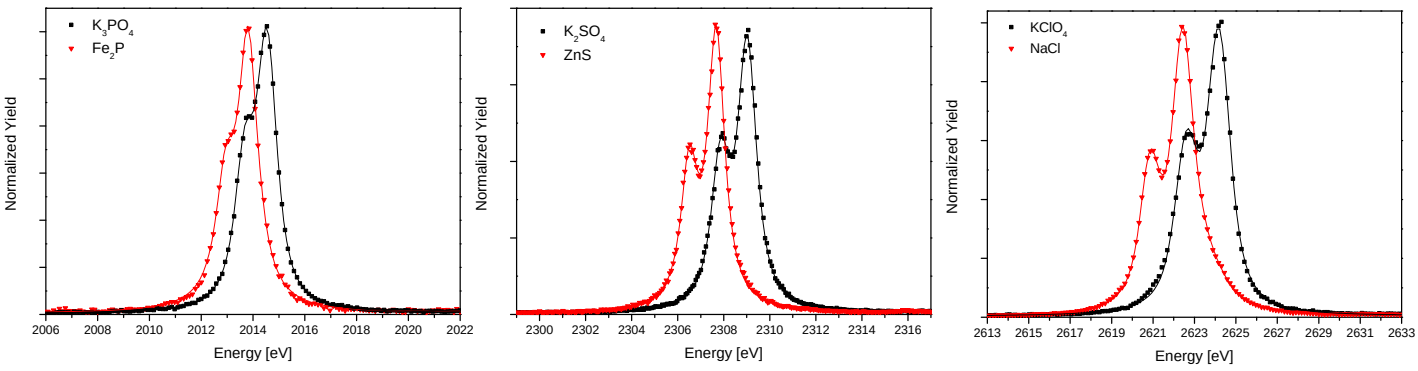

Fig. 1 High energy resolution proton induced $K\alpha_{1,2}$ X-ray emission spectra of two P, S, and Cl compounds corresponding to the lowest and the highest oxidation state.

Table 1 Experimental $K\alpha_1$ emission energies of various phosphorus, sulfur and chlorine compounds extracted from the fit.

Phosphorus			Sulfur			Chlorine		
chemical formula	oxidation state	$K\alpha_1$ [eV] measured	chemical formula	oxidation state	$K\alpha_1$ [eV] measured	chemical formula	oxidation state	$K\alpha_1$ [eV] measured
Fe_2P	3−	2013.81	FeS	2−	2307.71	$AlCl_3$	1−	2622.49
$CaH_4O_4P_2$	1+	2014.24	MoS_2	2−	2307.77	$CaCl_2$	1−	2622.47
Na_2HPO_3	3+	2014.43	PbS	2−	2307.71	CsCl	1−	2622.46
$Al(PO_3)_3$	5+	2014.61	ZnS	2−	2307.69	$CuCl_2$	1−	2622.54
$Ba(PO_3)_2$	5+	2014.52	pure S_8	0	2307.89	KCl	1−	2622.45
K_3PO_4	5+	2014.54	$Na_2S_2O_4$	3+	2308.33	$MgCl_2$	1−	2622.49
KH_2PO_4	5+	2014.51	$Na_2S_2O_5$	4+	2308.55	NaCl	1−	2622.44
Na_2HPO_4	5+	2014.55	Na_2SO_3	4+	2308.67	$KClO_3$	5+	2623.68
NaH_2PO_4	5+	2014.55	H_3NSO_3	5+	2308.97	$NaClO_3$	5+	2623.68
			$BaSO_4$	6+	2309.06	$KClO_4$	7+	2624.19
			$FeSO_4$	6+	2309.08			
			K_2SO_4	6+	2309.05			
			Na_2SO_4	6+	2309.07			

ments including the Na_2SO_3, $Na_2S_2O_5$ ones. The DFT valence electron populations show an increase of the effective electronic charge (number of valence electrons) for S atom within $Na_2S_2O_5$ compared to Na_2SO_3 compound. In Figure 4 the measured $K\alpha$ energies are plotted versus the DFT calculated number of valence electron. Compared to the dependence on formal oxidation number the degree of correlation between the two variables is enhanced even further and an almost perfect correlation is observed in this plot with the Na_2SO_3 and $Na_2S_2O_5$ compounds ordered directly in accordance with their calculated effective charge. The $K\alpha$ emission energy therefore reflects with high accuracy the valence electron population and can be used to determine the effective charge of the central low-Z atom in different chemical compounds.

5 Discussion

The $K\alpha$ emission spectra obtained in this work show clear dependence on the oxidation state of the element in the sample. As seen from the spectra presented in Fig. 1 the spectral shape of the $K\alpha_{1,2}$ emission line corresponding to core-core transition exhibit pure atomic-like $K\alpha_{1,2}$ doublet for all three studied elements inde-

Table 2 The DFT-calculated valence electron configuration obtained by the Mulliken population analysis. The notations in the superscript represent effective partial charges of the P, S and Cl atoms within the given molecule.

chemical formula	oxidation state	DFT electron configuration
Fe_2P	3−	$3s^{1.66}3p^{2.97}3d^{0.11}$
$CaH_4O_4P_2$	1+	$3s^{1.10}3p^{2.50}3d^{0.41}$
Na_2HPO_3	3+	$3s^{0.89}3p^{2.40}3d^{0.52}$
Na_2HPO_4	5+	$3s^{0.73}3p^{2.39}3d^{0.57}$
ZnS	2−	$3s^{1.87}3p^{4.16}3d^{0.03}$
$Na_2S_2O_5$	4+	$3s^{1.67}3p^{3.02}3d^{0.40}$
Na_2SO_3	4+	$3s^{1.67}3p^{2.89}3d^{0.38}$
K_2SO_4	6+	$3s^{1.05}3p^{3.03}3d^{0.66}$
NaCl	1−	$3s^{1.97}3p^{5.59}3d^{0.00}$
$KClO_3$	5+	$3s^{1.76}3p^{3.71}3d^{0.40}$
$NaClO_3$	5+	$3s^{1.76}3p^{3.69}3d^{0.40}$
$KClO_4$	7+	$3s^{1.31}3p^{3.57}3d^{0.68}$

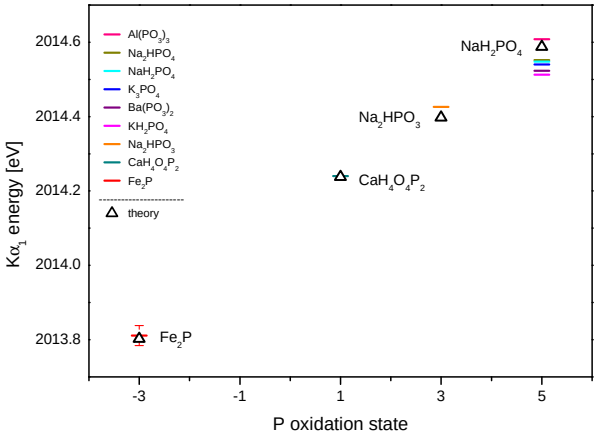

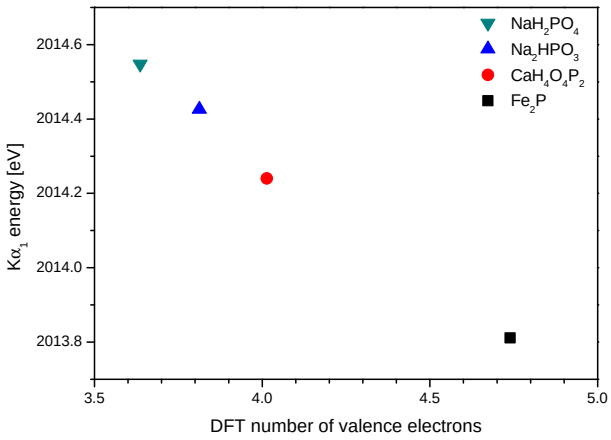

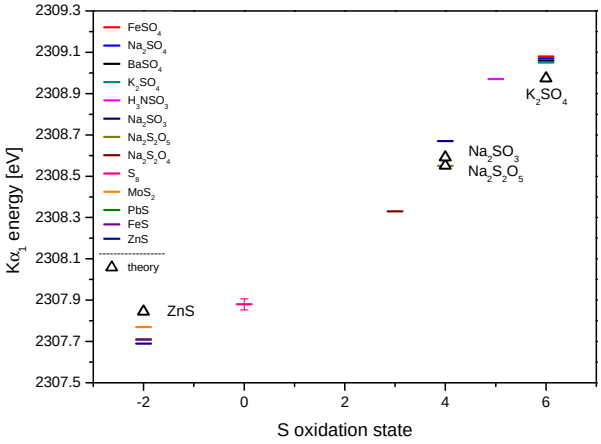

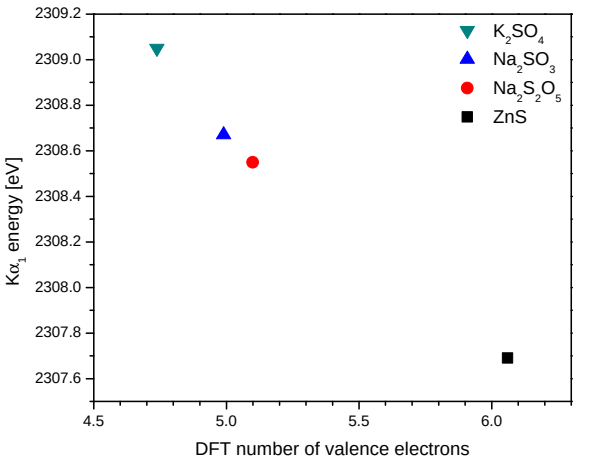

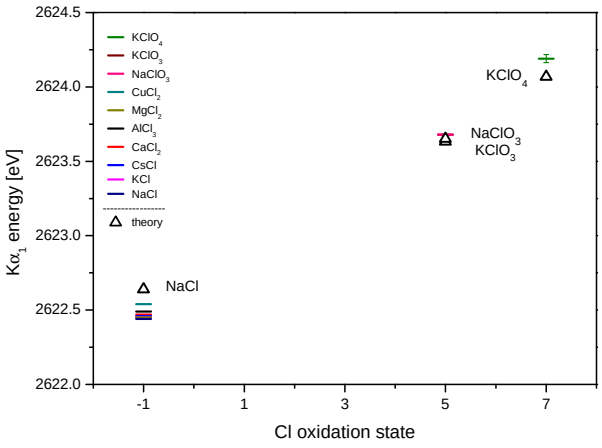

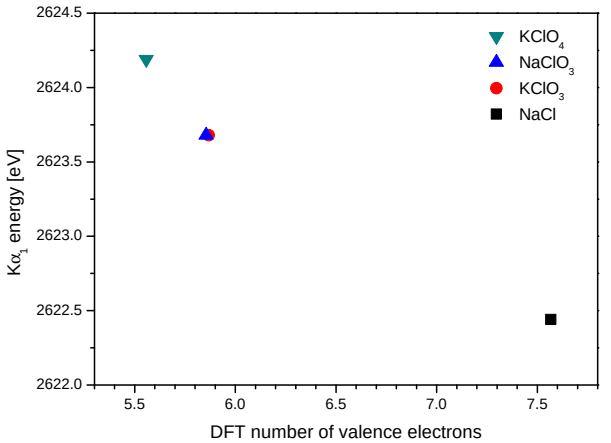

Fig. 3 Experimental and theoretical Kα_1 emission energies versus formal oxidation state.

Fig. 4 Experimental Kα_1 emission energies vs DFT calculated number of valence electrons.

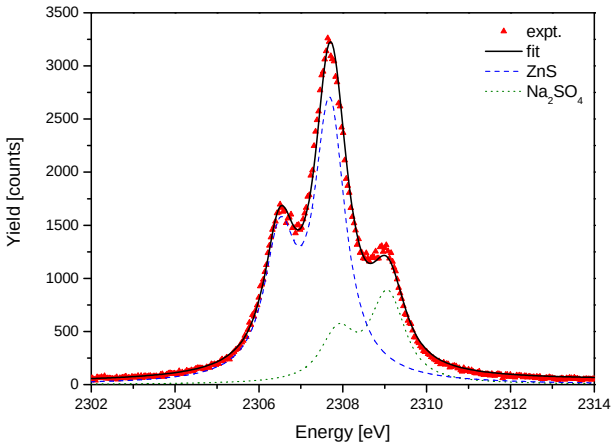

Fig. 5 S $K\alpha$ emission spectrum of ZnS / Na_2SO_4 mixed sample fitted with a linear combination of pure ZnS and Na_2SO_4 reference measured spectra.

pendent of the chemical composition. While the spectral shape is not influenced by the chemical environment the screening of the nuclear potential is affected by the valence orbital electron population and at high experimental resolution on the level of natural lifetime broadening tiny energy shifts of the measured $K\alpha$ emission lines are observed in correlation with the oxidation state of the element in the sample. The absolute energy shifts are relatively small, yielding values around 0.8, 1.3 and 1.7 eV between lowest and highest oxidation state in P, S and Cl, respectively, which is typically an order of magnitude smaller compared with the corresponding shifts measured in absorption spectra. However, due to the relatively simple and narrow line shape which in addition does not change with the chemical state the energy shift can be determined with very high precision and can be used effectively as a clean and robust merit of the oxidation state of these low-Z elements in the sample. Besides the dependence on formal oxidation state discussed above measured energy shifts are compared also to the effective local charge extracted from the quantum chemical calculations. In this case an almost perfect correlation is achieved between measured $K\alpha$ emission energies and DFT calculated number of valence electrons indicating that screening effects are prevailing source of the observed chemical sensitivity.

Compared to XANES, which is traditionally used for such analysis but generally contains more information than just the oxidation state, the energy of the $K\alpha$ emission line probes exclusively and directly the local charge density. Since its simple atomic-like shape is also independent on the excitation mode, as verified experimentally in our recent study of phosphorus comparing proton induced and synchrotron radiation induced K X-ray emission spectra [19], the method and results obtained here are generally relevant for X-ray emission spectroscopy using variety of excitation sources. It is important to note that in the synchrotron radiation community the tender X-ray range discussed in this work has been scientifically much less exploited then the soft and hard X-ray regions, mainly due to problems with X-ray optics and sample environment and it is not straightforward to find a proper beamline to measure for example phosphorus K edge XANES spectra. On the other hand, XES spectroscopy does not require monochromatic tunable incident photon beam and can be performed also at excitation energies well above the corresponding absorption edges. Using a good tender X-ray emission spectrometer such analysis can be therefore performed at many synchrotron beamlines as well as in smaller laboratories and the $K\alpha$ emission spectra can be fully exploited as the most sensitive probe of the local charge density of low-Z elements with emission energies in the tender X-ray range.

Good selectivity between different oxidation states together with relatively simple and narrow $K\alpha_{1,2}$ lineshape can be used to determine also the amount of particular species in mixed valence systems. Figure 5 shows the measured $K\alpha$ spectrum from mixed ZnS and Na_2SO_4 powder sample. This sample was prepared by mixing the pure ZnS and Na_2SO_4 powders in 2.5:1 molar quantity ratio so the corresponding mass percentage of sulfur in the S^{2-} oxidation state should be 71.4%. The measured spectrum was fitted with two Voigt doublets corresponding to the sulfur $K\alpha$ lines of pure ZnS and Na_2SO_4 compounds, with only relative areas of two doublets lines reflecting the ratio of the S^{2-} and S^{6+} in mixed sample set as a free parameter. Very good fit was obtained and both components corresponding to each chemical state were easily decomposed from the measured spectrum. The percentage of S^{2-} obtained from the fit was 73.4(2)%. The slight discrepancy between nominal and measured values can be attributed to the target self absorption. In general the self absorption does not influence the spectral shape of the X-ray emission spectra but only the overall yield. However, in case of heterogeneous powder samples with large grain size exceeding the X-ray absorption length, which is in case of $K\alpha$ MeV proton induced emission of P, S, and Cl between 10-20 μm, different self-absorption of separate single-compound grains might influence the overall accuracy of such mixed-valence compound systems. It is worthed to point out here that compared to other X-ray emission techniques PIXE yields an opportunity to observe simultaneously the depth distribution and give also a direct measure of inhomogeneity using the nuclear scattering necessarily accompanying the PIXE measurements [38].

Another important aspect in any X-ray analytical method is also the minimum detection limit (MDL). This is defined by the peak to background ratio and the width of the measured lines. From the fitting of our measured single compound spectra an average background level of 0.015 counts/s was determined. As an example the case of pure S target was considered yielding the count rate of 35 counts/s at the top of the sulfur $K\alpha_1$ line and the full width half maximum (FWHM) value of 0.87 eV. The corresponding detection limit was evaluated following the procedure used previously to determine MDL in HR-PIXE analysis [39]. At proton beam current in the range of 50-100 nA as used in our work and with acquisition time of 1 h final detection limit of < 200 ppm was obtained. However, in order to determine the $K\alpha$ emission energy with sufficient precision an order of magnitude higher concentrations would be typically required. The HR-PIXE oxidation state

analysis based on the $K\alpha$ emission energy is therefore applicable also on diluted samples with concentrations in the range of few 1000 ppm. Using other stronger and more efficient excitation sources especially synchrotron beamlines this can be pushed even further down in the range of a few hundreds of ppm.

6 Conclusions

High energy resolution $K\alpha$ X-ray proton induced emission spectra were measured for a series of phosphorus, sulfur, and chlorine containing compounds. Small energy shifts of emission lines were measured which are correlated with formal oxidation state and also effective local charge obtained with quantum chemical calculations based on density functional theory. Measured $K\alpha$ X-ray emission energies reflects with high sensitivity local electronic structure and can be used effectively to determine the oxidation state of low-Z elements in different chemical environments. Simple atomic-like $K\alpha_{1,2}$ spectral shape which does not depend on the chemical environment enables a relatively simple and robust spectral deconvolution in mixed valence systems and the oxidation state analysis can be performed also on diluted samples. Finally, the method is applicable not only to HR-PIXE technique but in general to high resolution $K\alpha$ X-ray emission spectroscopy regardless of the excitation mode. Such electronic structure analysis is therefore not restricted to synchrotron facilities but can be now fully exploited also in laboratory based analysis.

Acknowledgement

This work has been supported by Marie Curie Actions - Initial Training Networks (ITN) as an Integrating Activity Supporting Postgraduate Research with Internships in Industry and Training Excellence (SPRITE) under EC contract no. 317169. The authors acknowledge the support of the Slovenian Research Program P1-0112 and excellent assistance of the Microanalytical Center (MIC) team in preparation of protons beam.

References

1 U. Bergmann and S. P. Cramer, *Proc. SPIE*, 1998, **3448**, 198–209.

2 P. Glatzel, F. M. F. de Groot and U. Bergmann, *Synchrotron Radiat. News*, 2009, **22**, 12–16.

3 E. Kleymenov, J. A. van Bokhoven, C. David, P. Glatzel, M. Janousch, R. Alonso-Mori, M. Studer, M. Willimann, A. Bergamaschi, B. Henrich and M. Nachtegaal, *Rev. Sci. Instrum.*, 2011, **82**, 065107.

4 R. Alonso-Mori, J. Kern, D. Sokaras, T.-C. Weng, D. Nordlund, R. Tran, P. Montanez, J. Delor, V. K. Yachandra, J. Yano and U. Bergmann, *Rev. Sci. Instrum.*, 2012, **83**, 073114.

5 J. Szlachetko, M. Nachtegaal, E. de Boni, M. Willimann, O. Safonova, J. Sa, G. Smolentsev, M. Szlachetko, J. A. van Bokhoven, J.-C. Dousse, J. Hoszowska, Y. Kayser, P. Jagodzinski, A. Bergamaschi, B. Schmitt, C. David and A. Lucke, *Rev. Sci. Instrum.*, 2012, **83**, 103105.

6 D. Sokaras, T.-C. Weng, D. Nordlund, R. Alonso-Mori, P. Velikov, D. Wenger, A. Garachtchenko, M. George, V. Borzenets, B. Johnson, T. Rabedeau and U. Bergmann, *Rev. Sci. Instrum.*, 2013, **84**, 053102.

7 M. Kavčič, M. Budnar, A. Mühleisen, F. Gasser, M. Žitnik, K. Bučar and R. Bohinc, *Rev. Sci. Instum.*, 2012, **83**,.

8 T. Jach, N. Ritchie, J. Ullom and J. A. Beall, *Adv. X-ray Anal.*, 2007, **50**, 51–53.

9 M. A. Reis, P. C. Chaves and A. Taborda, *X-Ray Spectrom.*, 2011, **40**, 141–146.

10 M. Palosaari, K. Kinnunen, J. Julin, M. Laitinen, M. Napari, T. Sajavaara, W. Doriese, J. Fowler, C. Reintsema, D. Swetz, D. Schmidt, J. Ullom and I. Maasilta, *J. Low Temp. Phys.*, 2014, **176**, 285–290.

11 J. Diaz, E. Ingall, C. Benitez-Nelson, D. Paterson, M. D. de Jonge, I. McNulty and J. A. Brandes, *Science*, 2008, **320**, 652–655.

12 A. C. Leri, M. B. Hay, A. Lanzirotti, W. Rao and S. C. B. Myneni, *Anal. Chem.*, 2006, **78**, 5711–5718.

13 K. A. Evans, J. A. Mavrogenes, H. S. O'Neill, N. S. Keller and L.-Y. Jang, *Geochemistry, Geophysics, Geosystems*, 2008, **9**, 1525–2027.

14 M. Cotte, J. Susini, N. Metrich, A. Moscato, C. Gratziu, A. Bertagnini and M. Pagano, *Anal. Chem.*, 2006, **78**, 7484–7492.

15 M. U. M. Patel, I. Arčon, G. Aquilanti, L. Stievano, G. Mali and R. Dominko, *ChemPhysChem*, 2014, **15**, 894–904.

16 R. Alonso Mori, E. Paris, G. Giuli, S. G. Eeckhout, M. Kavčič, M. Žitnik, K. Bučar, L. G. M. Pettersson and P. Glatzel, *Anal. Chem.*, 2009, **81**, 6516–6525.

17 K. Maeda, A. Tonomura, H. Hamanaka and K. Hasegawa, *Nucl. Instrum. Meth. Phys. Res. B*, 1999, **150**, 124 – 128.

18 T. Tada, H. Fukuda, J. Hasegawa and Y. Oguri, *Spectrochim. Acta, Part B*, 2010, **65**, 46 – 50.

19 M. Petric, R. Bohinc, K. Bučar, M. Žitnik, J. Szlachetko and M. Kavčič, *Anal. Chem.*, 2015, **87**, 5632–5639.

20 M. Kavčič, A. Karydas and C. Zarkadas, *Nucl. Instrum. Meth. Phys. Res. B*, 2004, **222**, 601 – 608.

21 M. Kavčič, A. G. Karydas and C. Zarkadas, *X-ray Spectrom.*, 2005, **34**, 310–314.

22 K. Maeda, K. Hasegawa, H. Hamanaka, M. Maeda, S. Yabuki and K. Ogiwara, *Nucl. Instrum. Meth. Phys. Res. B*, 2002, **190**, 704 – 708.

23 S. Wonglee, T. Tada, H. Fukuda, J. Hasegawa and Y. Oguri, *Nucl. Instrum. Meth. Phys. Res. B*, 2011, **269**, 3111 – 3114.

24 Z. Kertész, E. Furu and M. Kavčič, *Spectrochim. Acta, Part B*, 2013, **79 - 80**, 58 – 62.

25 M. Fichter, *Spectrochim. Acta Part B*, 1975, **30**, 417 – 431.

26 R. D. Deslattes, E. G. Kessler, P. Indelicato, L. de Billy, E. Lindroth and J. Anton, *Rev. Mod. Phys.*, 2003, **75**, 35–99.

27 K. Hermann, L. Pettersson, M. Casida, C. Daul, A. Goursot, A. Koester, E. Proynov, A. St-Amant, D. Salahub., V. Carravetta, H. Duarte, C. Friedrich, N. Godbout, J. Guan, C. Jamorski, M. Leboeuf, M. Leetmaa, M. Nyberg, S. Patchkovskii, L. Pedocchi, F. Sim, L. Triguero and A. Vela., *StoBe-deMon version 3.1*, 2011.

28 W. Kohn, *Rev. Mod. Phys.*, 1999, **71**, 1253–1266.

29 R. S. Mulliken, *J. Chem. Phys.*, 1955, **23**, 1833–1840.

30 R. S. Mulliken, *J. Chem. Phys.*, 1955, **23**, 1841 – 1846.

31 R. S. Mulliken, *J. Chem. Phys.*, 1955, **23**, 2338–2342.

32 R. S. Mulliken, *J. Chem. Phys.*, 1955, **23**, 2343–2346.

33 A. Nilsson and L. G. M. Pettersson, *Surf. Sci. Rep.*, 2004, **55**, 49–167.

34 A. Föhlisch, J. Hasselström, P. Bennich, N. Wassdahl, O. Karis, A. Nilsson, L. Triguero, M. Nyberg and L. G. M. Pettersson, *Phys. Rev. B*, 2000, **61**, 16229–16240.

35 A. Becke, *Phys. Rev. A*, 1988, **38**, 3098–3100.

36 J. Perdew and Y. Wang, *Phys. Rev. B*, 1992, **45**, 13244–13249.

37 J. Perdew, J. Chevary, S. Vosko, K. Jackson, M. Pederson, D. Singh and C. Fiolhais, *Phys. Rev. B*, 1992, **46**, 6671–6687.

38 C. Jeynes, M. Bailey, N. Bright, M. Christopher, G. Grime, B. Jones, V. Palitsin and R. Webb, *Nucl. Instrum. Meth. Phys. Res. B*, 2012, **271**, 107 – 118.

39 M. Kavčič, *Nucl. Instrum. Meth. Phys. Res. B*, 2010, **268**, 3438 – 3442.

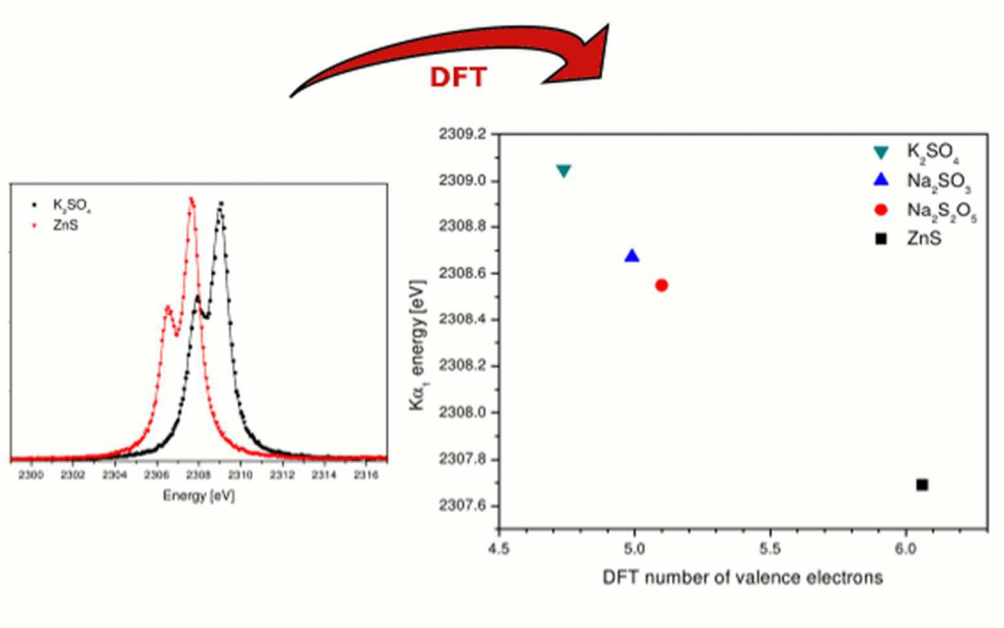

200x124mm (72 x 72 DPI)